Eur. Phys. J. D **41**, 363–369 (2007)
DOI: 10.1140/epjd/e2006-00223-y

THE EUROPEAN PHYSICAL JOURNAL D

Frequency degenerate and non-degenerate nonlinear regimes for semi-linear photorefractive oscillator

M. Grapinet[1], P. Mathey[1,a], H.R. Jauslin[1], B. Sturman[2], D. Rytz[3], and S. Odoulov[4]

[1] Laboratoire de Physique de l'Université de Bourgogne, UMR CNRS 5027, 9 avenue A. Savary, B.P. 47870, 21078 Dijon, France
[2] Institute of Automation and Electrometry, Russian Academy of Sciences, 630090 Novosibirsk, Russia
[3] Forschunginstitute für mineralische and metallische Werkstoffe, Edelsteine/Edelmetalle GmBH, Struhtstrasse 2, Wackenmuhle, 55743 Idar-Oberstein, Germany
[4] Institute of Physics, National Academy of Sciences, 252650 Kiev, Ukraine

Received 25 April 2006 / Received in final form 11 September 2006
Published online 29 September 2006 –

Abstract. We present a theoretical analysis, analytical and numerical, of the oscillation regimes for the semi-linear photorefractive oscillator beyond the instability threshold. This analysis includes the limiting cases of dominating transmission and reflection gratings as well as the cases of spontaneous violation of the frequency degeneracy between the oscillation and pump waves.

PACS. 42.65.Hw Phase conjugation; photorefractive and Kerr effects – 05.45.-a Nonlinear dynamics and chaos – 42.65.Pc Optical bistability, multistability, and switching, including local field effects – 42.65.Sf Dynamics of nonlinear optical systems; optical instabilities, optical chaos and complexity, and optical spatio-temporal dynamics

1 Introduction

Strong photorefractive (PR) nonlinearity inherent in electro-optic materials (in particular, ferroelectrics and semiconductors) has led to the emergence of numerous optical schemes employing the advantages of the phase conjugation and optical oscillation [1–5]. The so-called semi-linear oscillator was one the first nonlinear devices of this type [6]. Its cavity is formed by an ordinary feedback mirror and a photorefractive crystal that serves as an amplifying phase-conjugate mirror pumped by two counter-propagating coherent light waves of the same frequency, see Figure 1. Owing to its apparent simplicity, this scheme serves often as a sample for investigation of dynamic properties of PR oscillators, including the threshold behavior, bifurcations with increasing supercriticality, and transition to chaos [7–10].

The operation of the semi-linear oscillator is based on buildup of refractive index gratings (by different pairs of pump and oscillation waves) and diffraction from these gratings. By playing with the coherence length and/or material properties, one can realize the distinct cases of transmission and reflection gratings, see Figures 1a and 1b. The basic dynamic equations for these cases are well-known [2,3]. For the most common diffusion photorefractive response and frequency degenerate oscillation, these nonlinear equations admit exact steady-state solutions incorporating the effect of pump depletion [3,11]. In the transmission (T) case, these exact solutions correspond to the soft and hard excitation scenarios for different areas of the pump ratio r and the feedback mirror reflectivity R. In the reflection (R) case, the exact solutions correspond to the soft threshold behavior.

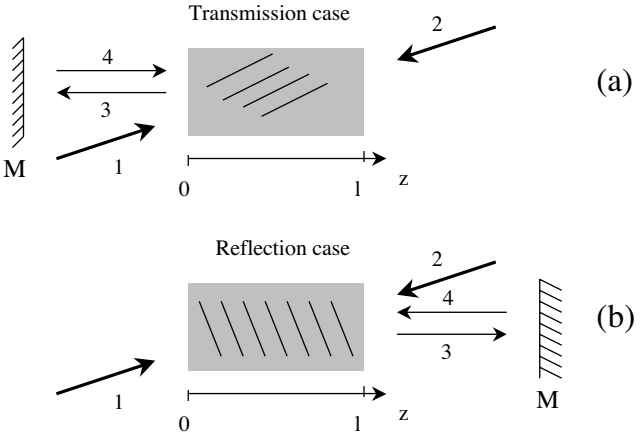

Fig. 1. Schematic diagram of the semi-linear photorefractive oscillator for the cases of dominating transmission (a) and reflection (b) grating; M is the ordinary feedback mirror and l is the crystal thickness.

Experiment shows [12,13] that changing pump ratio can result in a frequency bifurcation of the oscillation

[a] e-mail: pmathey@u-bourgogne.fr

mode for the diffusion photorefractive response: the single-frequency oscillation transforms into a two-frequency oscillation. An explanation of this phenomenon was given first on the basis of a heuristic analysis of the influence of the frequency splitting on the oscillation threshold [12–14] whose key point is the assumption of an automatic fulfillment of phase matching for the oscillation wave during a round trip in the cavity. Recently we presented a full-scale analysis of the threshold and above-threshold behavior of the semi-linear oscillator within the undepleted pump approximation for the transmission case and diffusion nonlinear response [16]. It is based on the conventional basic dynamic equations for the wave and grating amplitudes and incorporates both the intensity and phase matching for the oscillation waves. The results of this analysis are fully applicable also to the case of dominating reflection grating. They contrast with the predictions of the heuristic model.

In this paper, we present the results of our analytical and numerical studies of the oscillation regimes beyond the undepleted pump approximation. They include the indication of the regions of the control parameters where the oscillation is frequency degenerate and non-degenerate, a quantitative characterization of the both oscillation regimes, and comparison between the cases of dominating transmission and reflection gratings.

2 Basic equations and oscillation instability

The initial set of equations for the semi-linear oscillator in the T and R cases, which corresponds to Figures 1a and 1b, can be presented in the following uniform form [2,3]:

$$\frac{\partial A_1}{\partial z} = \nu^* A_4 \tag{1}$$

$$\frac{\partial A_2}{\partial z} = \nu A_3 \tag{2}$$

$$\frac{\partial A_3}{\partial z} = s\nu^* A_2 \tag{3}$$

$$\frac{\partial A_4}{\partial z} = s\nu A_1 \tag{4}$$

$$t_r \frac{\partial \nu}{\partial t} + \nu = \frac{\gamma}{I_0}\left(A_1^* A_4 + A_2 A_3^*\right) . \tag{5}$$

Here $A_{1,2,3,4}$ are the amplitudes of light waves 1, 2, 3, 4, ν is the grating amplitude, γ is a real coupling constant, $I_0 = I_1 + I_2 + I_3 + I_4$ is the total intensity, $I_i = |A_i^2|$ is the intensity of the ith wave, $t_r \propto 1/I_0$ is the photorefractive response time, and the asterisk stands for complex conjugation. Parameter s equals -1 for the transmission case and $+1$ for the reflection case.

The boundary conditions for pump waves 1 and 2 are $A_1(0,t) = A_1^0 = const$, $A_2(l,t) = A_2^l = const$. The boundary conditions for the oscillation waves 3 and 4 are slightly different for the T and R cases, see Figure 1,

$$\begin{aligned} &A_3(l,t) = 0, \quad A_4(0,t) = \sqrt{R}\, A_3(0,t) \quad \text{T case} \\ &A_3(0,t) = 0, \quad A_4(l,t) = \sqrt{R}\, A_3(l,t) \quad \text{R case}, \end{aligned} \tag{6}$$

where l is the crystal thickness and R is the reflection coefficient of the feedback mirror M.

Within the undepleted pump approximation (the linear approximation in $A_{3,4}$) we can discard equations (1) and (2) for the pump waves and set $A_1 = A_1^0, A_2 = A_2^l$ in equations (3–5). Then the difference between the T and R cases comes from the sign $s = \pm 1$ and from the boundary conditions (6). Making a spatial inversion with respect to the crystal center ($z = l/2$) in the R case one can eliminate even this difference. Thus, the results obtained within the undepleted pump approximation are the same for the transmission and reflection cases.

The ansatz relevant to the instability analysis within the undepleted pump approximation has the form

$$\begin{aligned} A_{3,4}(z,t) &= \left[A_{3,4}^+(z)\, e^{i\Omega t} + A_{3,4}^-(z)\, e^{-i\Omega t}\right] e^{pt} \\ \nu(z,t) &= \left[\nu^+(z)\, e^{i\Omega t} + \nu^-(z)\, e^{-i\Omega t}\right] e^{pt} , \end{aligned} \tag{7}$$

where Ω is the frequency detuning, p is the rate of temporal growth (the increment), whereas $A_{3,4}^{\pm}(z)$ and $\nu^{\pm}(z)$ are certain spatial amplitudes meeting the relevant coupled-wave equations and boundary conditions. The final complex dispersion equation, which is applicable both to the T and R cases, reads:

$$\frac{g}{1 + p\, t_r - i\Omega t_r} = L_{\pm} , \tag{8}$$

where $g = \gamma l$ is the coupling strength and $L_{\pm} = \ln\left[(\sqrt{rR} \pm r)/(\sqrt{rR} \mp 1)\right]$ is a known function of the beam ratio $r = I_2^l/I_1^0$ and reflection coefficient R. It is understood according to the definition of the logarithmic function of a complex variable Z, $\ln Z = \ln|Z| + i\arg(Z)$. The signs + and − in this equation correspond to two independent solutions for $p(r,R)$ and $\Omega(r,R)$.

The main outcomes of the dispersion equation can be formulated as follows: for sufficiently low coupling strength, $|g| \lesssim 1.76$, we have $p < 0$ and $\Omega = 0$. In other words, small perturbations of $A_{3,4}$ and ν decrease exponentially and monotonically in time and oscillation is not possible for any r and R. For the coupling strength within the range $1.76 \lesssim g < 2\pi$, the increment p is positive within a certain region of r, R while $\Omega = 0$. This corresponds to non-degenerate oscillations. For $g > 2\pi$ two new solutions of equation (8) with $p > 0$ become possible within two new regions of r, R; each of these new solutions for p corresponds to $\Omega = \pm|\Omega| \neq 0$, i.e., to a frequency degenerate oscillation. To consider the case $g < 0$, it is sufficient to mention that $L_{\pm}(r,R) = -L_{\mp}(r^{-1},R)$ in equation (8); therefore we have $p(g,r,R) = p(-g,r^{-1},R)$, $|\Omega|(g,r,R) = |\Omega|(-g,r^{-1},R)$.

Figure 2 shows the functions $p(r)$ and $|\Omega|(r)$ for $g = 7$ and $R = 0.01$. One sees that the value $[p(r)]_{max}$ is the same for the frequency degenerate branches 1 and 2 and it is comparable with $[p(r)]_{max}$ for the non-degenerate branch 0. The middle branch 1 is overlapping with the left and right branches so that there are intervals of r where one and two types of instabilities can take place simultaneously. For curve 0 we have $\Omega \equiv 0$, whereas for curves 1 and 2 the frequency detuning acquires nonzero

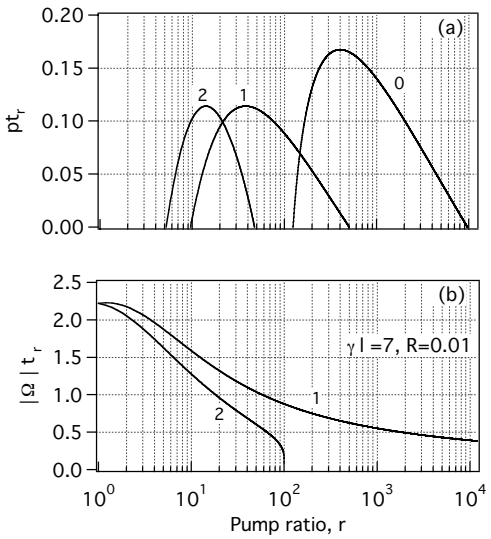

Fig. 2. Dependence of the increment p and the absolute value of frequency detuning $|\Omega|$ on the pump ratio r for $g = 7$ and $R = 0.01$; curve 0 corresponds to the frequency degenerate oscillation while curves 1 and 2 are plotted for solution of equation (8) with $\Omega \neq 0$.

values in the whole interval of r where $p > 0$. Note that $|\Omega|(r)$ turns to zero very abruptly near the end of branch 2 and also that branches 0 and 2 are well separated; this is the general feature coming from equation (8).

The behavior of p and $|\Omega|$ with changing g is quite evident from equation (8); with decreasing coupling strength the regions where $p > 0$ shrink for branches 1 and 2, so that branch 0 becomes dominating and the overlaps between different instability regions disappear. The effect of changing R is not so evident. It can be commented as follows: When R is increasing, the value of $[p(r)]_{max}$ increases quicker for branch 0 then for branches 1 and 2, this degenerate branch becomes thus dominating. Furthermore, branches 1 and 2 become more and more horizontally separated. Because of that, curve 1 lays below curve 0 for $p > 0$. With decreasing reflection coefficient, the value $[p(r)]_{max}$ becomes negative for branch 0; the degenerate instability disappears, at $R \lesssim 3.6 \times 10^{-3}$. For $R \to 0$, the branches 1 and 2 confluence which corresponds to the mirrorless oscillation [3,15].

Thus, for the parameters of Figure 2 we have the most general and interesting situation with five qualitatively different regions of instability. Different oscillation modes are expected to compete in these regions. Consideration of developed oscillations is indeed beyond the undepleted pump approximation and analytical treatments.

The linearized theory, when applicable, gives also useful predictions with regard to the arguments (phases) of the complex amplitudes of the oscillation waves for different modes of instability. In particular, we have: $\mathrm{Re}A_3 \propto \exp(p_0 t)$, $\mathrm{Im}A_3 = 0$ for mode 0; $\mathrm{Re}A_3(t) = 0$, $\mathrm{Im}A_3 \propto \exp(p_1 t)\cos(\Omega_1 t + \varphi_1)$ for mode 1; and $\mathrm{Re}A_3 \propto \exp(p_2 t)\cos(\Omega_2 t + \varphi_2)$, $\mathrm{Im}A_3 = 0$ for mode 2, where $\varphi_{1,2}$ are some constants that are of no interest for what follows. Strictly speaking, this particular presentation is valid for real input pump amplitudes A_1^0 and A_2^l. In the general case, a trivial re-normalization $A_3 \to A_3 \exp(i\phi)$ with a time-independent phase ϕ is sufficient to use the above results.

3 Numerical procedure

To simulate the temporal development of the optical oscillations for different values of the pump ratio r, we have used a finite difference scheme to solve the system (1–5) of nonlinear partial differential equations, written in a normalized (dimensionless) form. The amplitudes $A_{1,4}$ and $A_{2,3}$ are normalized to the boundary values of the pump amplitudes A_1^0 and A_2^l, respectively, in accordance with the structure of the initial set and Figure 1. The propagation coordinate z is normalized to the crystal thickness l. The dimensionless grating amplitude is νl. The time t is normalized to the response time $t_r^0 = t_r\, I_0/(I_1^0 + I_2^l)$ calculated for the total input pump intensity. The initial values (at $t = 0$) of the oscillation amplitudes $A_{3,4}$ are set to be zero while the initial value of νl, is chosen in the form of a complex random function whose absolute value does not exceed 10^{-4}. This seed initiates the instability but, as we have checked, does not influence either its linear stage or the steady state.

It should be emphasized that our numerical procedure does not impose particular values of the frequency detuning. The time behavior of the amplitudes is fully determined by the structure of the basic nonlinear equations.

4 Frequency degenerate and non-degenerate oscillations

Despite the fact that the behavior of the semi-linear oscillator in the T and R cases is the same within the undepleted pump approximation, the steady state oscillations in these cases are different. This reflects indeed the difference in the complete set of starting equations (1–5) for the cases $s = +1$ and -1.

In what follows, we provide the reader not only with time dependences of the oscillation intensity $I_3 = |A_3|^2$ but also with time dependences of the real and imaginary parts of the oscillation amplitude A_3. This allows to see the development and stabilization of the oscillation instability in detail. The time intervals to be shown are sufficient to demonstrate the most remarkable features of the oscillation dynamics; generally, we performed numerical calculations over much longer intervals.

4.1 Transmission case

To understand the relationship between the degenerate and non-degenerate oscillations, we will analyze the case $g = 7$, $R = 0.01$ considered in the previous section. It is characterized by competition between different regimes and also by the presence of several distinct regions of the pump ratio.

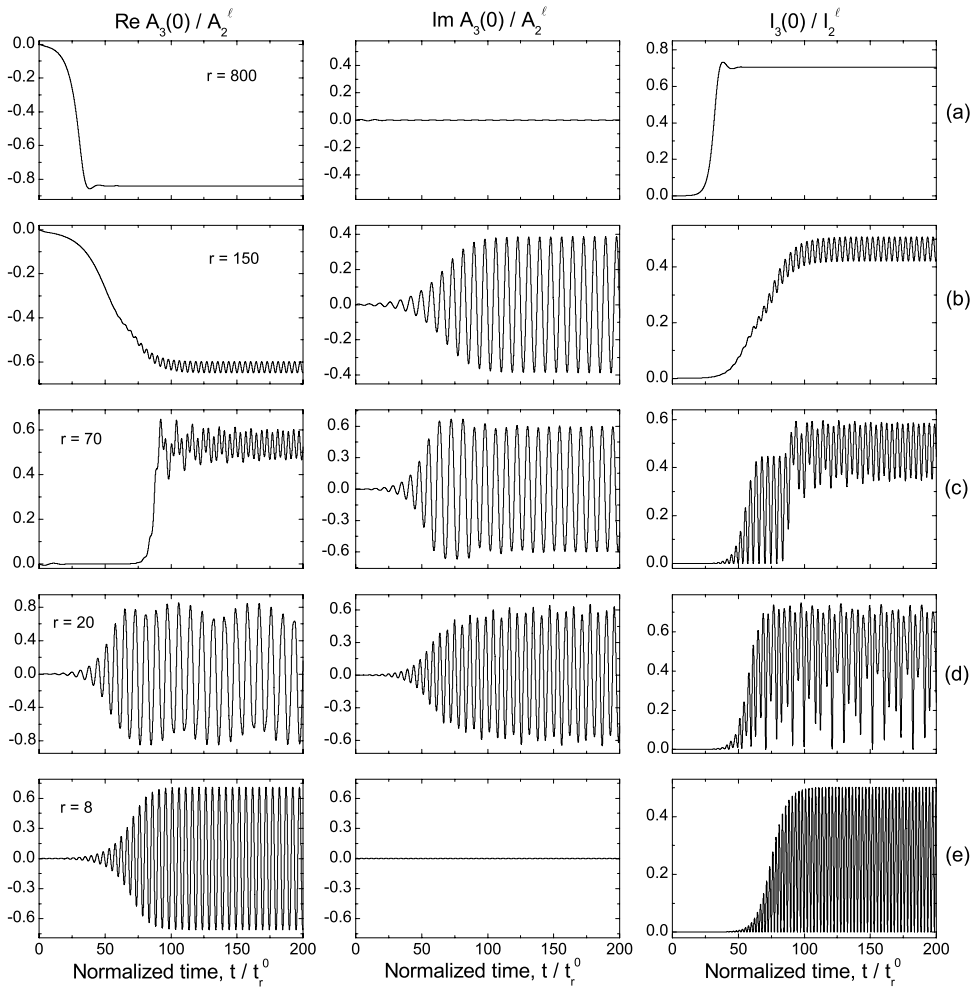

Fig. 3. Oscillation dynamics versus the pump ratio r for the coupling strength $g = 7$ and the reflectivity $R = 0.01$ in the transmission case. The sub-figures (a) to (e) correspond the values of the pump ratio $r = 800$, 150, 70, 20, and 8. The first, second, and third rows refer to the normalized values of $\mathrm{Re}A_3(z = 0, t)$, $\mathrm{Im}A_3(z = 0, t)$, and $I_3(z = 0, t)$, respectively.

We set first $r = 800$, which corresponds to the instability with $\Omega = 0$ (branch 0) and to a pretty large value of the increment, $p\,t_r^0 \simeq 0.15$, see Figure 2a. The output oscillation intensity $I_3(0,t) = [\mathrm{Re}\,A_3(0,t)]^2$ first grows exponentially according to the linearized theory and arrives then (not quite monotonically) at the steady-state value that corresponds to the known exact solution for the degenerate oscillation ($\Omega = 0$), see Figure 3a. The imaginary part of the oscillation amplitude, $\mathrm{Im}\,A_3(0,t)$, remains zero not only during the initial stage of instability, which follows from the linearized theory, but also in the steady state. The steady-state value of $I_3(0)$ is pretty high; saturation of the instability is caused by the pump depletion.

Similar behavior is typical for the whole range $5\times10^2 \lesssim r \lesssim 10^4$ where the sole instability with $\Omega = 0$ takes place, see Figure 2. Moreover, even in the region $2.5\times10^2 \lesssim r \lesssim 5\times10^2$, where the degenerate mode 0 already co-exists with the non-degenerate mode 1, the oscillation remains almost frequency degenerate owing to the mode competition. Since frequency degenerate perturbations grow relatively fast, they suppress the non-degenerate mode on an early stage of the instability.

For $r \lesssim 200$, when the increment $p_1(r)$ becomes comparable with $p_0(r)$, the oscillation behavior changes. This is illustrated by Figure 3b for $r = 150$. An exponential growth of $\mathrm{Im}\,A_3(0)$, which is accompanied by oscillations and corresponds to the non-degenerated instability, becomes noticeable. Owing to nonlinear coupling, it affects the temporal development of $\mathrm{Re}\,A_3(0)$; the latter is characterized by oscillations at the double frequency. The output intensity $I_3(0)$ also experiences oscillations at the double frequency [as compared to that of $\mathrm{Im}\,A_3(0,t)$]; its oscillating part is noticeable not only in the steady state but also during the initial stage.

At $r = 150$, the steady-state oscillation period of $\mathrm{Im}A_3(0,t)$, $T \simeq 8.3t_r^0$, differs slightly from the value $2\pi/\Omega \simeq 7.9t_r^0$ prescribed by the dispersion equation (8); this implies that stabilization of the non-degenerate instability is caused by the nonlinear frequency shift. With a good accuracy, the output oscillation wave 3 can be characterized by the amplitude $A_3(0,t) \simeq -0.6 + 0.4i\cos(2\pi t/T)$ in the steady state. Smallness of the higher Fourier harmonics means that the nonlinear coupling between different modes is rather weak. When approaching the boundary of the degenerate instability region ($r \simeq 115$), the oscillating part of $A_3(0,t)$ (and that of $I_3(0,t)$) is monotonically increasing.

What happens in the range $45 \lesssim r \lesssim 115$ where the only possible instability corresponds to a frequency non-degenerate oscillation (mode 1)? On the basis of

the linearized theory one might expect that the constant parts of $A_{3,4}$ are zero and the oscillation intensities oscillate between zero and certain maximum values. This is not, however, the actual case, see Figure 3c. In reality, the system follows the linearized theory predictions only during an initial stage of development, namely for $t/t_r^0 \lesssim 90$. After that an abrupt transition to a new oscillation regime with relatively shallow intensity oscillations takes place. The described behavior is typical for the whole range of r indicated above. For $r = 70$, which corresponds to Figure 3c, the oscillation amplitude is $A_3(0,t) \simeq 0.53 - 0.62i\cos(2\pi t/T)$ in the steady state; the period $T \simeq 8.1t_r^0$ differs remarkably from the value $\simeq 6.58t_r^0$ prescribed by equation (8). The non-oscillating real part of $A_3(0,t)$ develops with a rather big delay and its sign is now positive. This points at a strong coupling between the oscillating and non-oscillating components of the beams.

The most complicated oscillation regimes occur within the interval $10 \lesssim r \lesssim 45$, where the two frequency non-degenerate modes compete with each other, see Figure 2a. It turns out that none of them generally dominates. This means that two-periodic steady-state oscillations take place. Figure 3d gives a representative example of such an optical oscillation; it corresponds approximately to the point of intersection of branches 1 and 2 where $p_1 \approx p_2$. Both real and imaginary parts of $A_3(0)$ are present here in full scale.

The last distinct interval of the pump ratio is $5 \lesssim r \lesssim 10$. Only a single non-degenerate oscillation mode 2 is admitted here within the linear theory, see Figure 2. The typical oscillation regime within this interval is presented in Figure 3e, it corresponds to $r = 8$. One sees that intensity $I_3(0,t)$ oscillates in steady state between zero and a modest maximum value. The amplitude $A_3(0,t)$ is real here; it equals approximately $0.74\cos(2\pi t/T)$ with a period $T \simeq 5.1t_r^0$ which is not far from the value $\simeq 4.3t_r^0$ prescribed by the linearized theory.

A surprising general feature of the above considered oscillation regimes is the smallness of the higher temporal Fourier harmonics of the oscillation amplitudes (with periods $T/2, T/3, \ldots$) as compared to the first harmonic(s). This means that the effects of nonlinear coupling are weak in a certain sense. At the same time, the oscillation amplitudes can be comparable with the amplitude of the strongest pump wave. These observations can facilitate analytical modelling of the oscillation regimes.

In the steady state, the main effect of decreasing r, when passing the above considered regions, is increasing fraction of the oscillation part of $I_3(t)$ (from 0 to 1).

4.2 Reflection case

Despite the fact that the linearized theory predicts the same for the R- and T-cases, the corresponding steady-state (and even transient) characteristics are different in many respects. Let us start again with the case $r = 800$, which corresponds to the region of frequency degenerate oscillations in Figure 2. In this range, the difference between the R- and T-cases is rather small. As one can see from Figure 4a, the oscillation intensity $I_3(l)$ grows in the R-case monotonically from noise to a constant steady-state value which is slightly lower than that in the T-case (compare with Fig. 3a). In contrast to the T-case, the sign of $\mathrm{Re}A_3$ is positive.

In the region $115 \lesssim r \lesssim 7 \times 10^2$, where the increment of the instability p is positive for both branches 0 and 1, we have a qualitatively new behavior. It is represented by Figure 4b for $r = 220$. The real part of the amplitude $A_3(l)$ and the intensity $I_3(l)$ grow first monotonically with the increments p_0 and $2p_0$, respectively, to arrive at intermediate quasi-steady-state values corresponding to the frequency degenerate oscillation. The imaginary part of $A_3(l)$ remains relatively small at this stage. However, this intermediate steady state is not stable because of oscillatorily increasing $\mathrm{Im}A_3(l,t)$. Finally, after a relatively long transient stage, the system arrives at a true steady state which is characterized by strong oscillations of $I_3(l)$ around an average value of $\simeq 0.4$. The steady-state amplitude of wave 3 is given by $A_3(l) \simeq 0.39 + 0.076\cos(4\pi/T) + 0.72i\cos(2\pi/T)$, where the period $T \simeq 13.95\,t_r^0$ is noticeably different from the value $\simeq 8.55$ prescribed by the linearized theory. Weak forced oscillations of $\mathrm{Re}A_3$ at the double frequency are fully due to the nonlinear coupling effects.

With decreasing pump ratio, the intermediate stage becomes shorter (because of increasing increment $p_1(r)$) while the subsequent drop of $\mathrm{Re}A_3(l)$ becomes more and more pronounced. Near the lower border of the degenerate instability region, $r = 130$–160, the non-degenerate mode of oscillation becomes dominating. This is illustrated by Figure 4c for $r = 150$. A modest influence of the degenerate instability can be seen only during a short initial stage. The steady state is characterized here by an almost 100% modulation contrast and by the amplitude $A_3(l) \simeq 0.93i\cos(2\pi t/T)$ with the period $T \simeq 13t_r^0$. This period is noticeably larger again compared to that, $\simeq 7.9t_r^0$, calculated from the linearized theory.

Within the range $45 \lesssim r \lesssim 115$, where the increment of instability is positive only for branch 1, development of the oscillation is fairly simple. The real part of A_3 remains negligible while the imaginary part, $\mathrm{Im}A_3(l)$, grows oscillatorily until the steady state with a 100% intensity modulation contrast. It is interesting that the period of oscillations grows gradually from the value prescribed by the linearized theory to a considerably larger steady-state value. This effect is not influenced here by the degenerate mode of instability which points at stabilization of the instability by the nonlinear frequency shift.

The range $10 \lesssim r \lesssim 45$, where both increments $p_{1,2}$ are positive, is characterized by a strong competition of the corresponding modes of instability. The result of this competition is determined, roughly speaking, by the ratio $p_1(r)/p_2(r)$. When this ratio is larger than one ($r > 20$, see Fig. 2), the modes of instability 1 and 2, which are presented by $\mathrm{Im}A_3(l,t)$ and $\mathrm{Re}A_3(l,t)$, respectively, coexist only during an initial stage of instability. Afterwards,

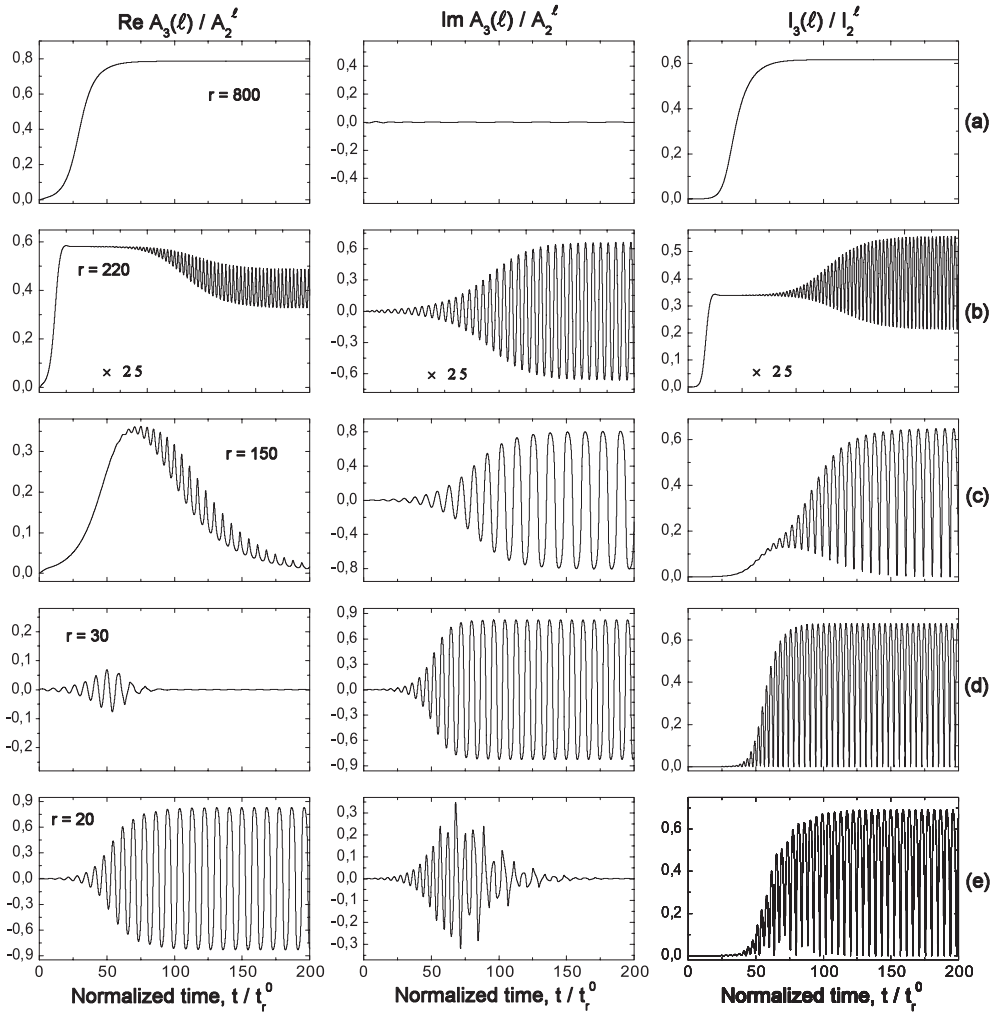

Fig. 4. Oscillation dynamics versus the pump ratio r for the coupling strength $g = 7$ and the reflectivity $R = 0.01$ in the reflection case. The sub-figures (a) to (e) correspond the values of the pump ratio $r = 800$, 220, 150, 30, and 20. The first, second, and third rows refer to the normalized values of $\mathrm{Re}A_3(z = l, t)$, $\mathrm{Im}A_3(z = l, t)$, and $I_3(z = l, t)$, respectively. Note that the time interval in the case (b) is 2.5 times longer than for the other cases.

development of mode 1 suppresses mode 2 and the steady-state amplitude $A_3(l, t)$ is pure imaginary. For $r \lesssim 20$, the roles of modes 1 and 2 are opposite and the steady state amplitude $A_3(l, t)$ is purely real. This is illustrated by Figures 4d and 4e. Steady-state intensity characteristics (the averaged value, the contrast, and the period) do not experience dramatic changes in the vicinity of $r = 20$.

When the pump ratio r decreases from $\simeq$10 to $\simeq$5, the transient stage of oscillation, which is controlled by mode 2, becomes longer and longer while the steady-state oscillation amplitude and intensity tend to zero according the usual soft-excitation scenario. For $5 \lesssim r$, the oscillation is absent in agreement with the linearized theory.

5 Summary

Investigating analytically and numerically the conventional set of nonlinear equations for the semi-linear photorefractive oscillator, we have found a wealth of different oscillation regimes for sufficiently large values of the coupling strength, $g > 2\pi$. These nonlinear regimes are characterized by the frequency degenerate and/or non-degenerate oscillations, and also by the co-existence and/or competition of different oscillation modes. The found nonlinear behavior is essentially different for the principal schemes employing the transmission and reflection gratings. Our findings fill the gap in the knowledge of the oscillation regimes of the semi-linear oscillators, which has so far been restricted to the frequency degenerate case. They also contribute to the basics of nonlinear dynamics because the basic nonlinear equations are fairly general and simple.

Several particular outcomes of our theory are worth mentioning:

- within the intervals of the pump ratio where the linearized theory predicts the frequency degenerate instability, the steady-state oscillations always remain degenerate;
- frequency degenerate and non-degenerate oscillation modes, predicted by the linear analysis [16], co-exist in the steady state within certain intervals of the control parameters, which results in periodic, contrast-variable modulation of the output intensities;
- within certain ranges of the control parameters, the mode competition results in survival (in the steady state) only one oscillation mode;

– the relative values of the increments of the instability for the oscillation modes, which are predicted by the linearized theory [16], are crucially important in the case of mode competition; the mode with the strongest increment typically wins the competition;
– nonlinear frequency shifts for the non-degenerate oscillation waves play an important role in stabilization of the instability;
– temporal oscillations of the wave amplitudes are typically almost harmonic in steady state, i.e., the high-order nonlinear coupling effects are small;
– the phases of the oscillation waves do not experience strong nonlinear changes, i.e., the relationships between the real and imaginary components of the oscillation amplitudes roughly concise with those prescribed by the linear theory.

B.S. and S.O. acknowledge the hospitality as invited professors at Université de Bourgogne.

References

1. M. Cronin-Golomb, B. Fisher, J.O. White, A. Yariv, IEEE J. Quantum Electron. **QE-20**, 12 (1984)
2. S. Kwong, M. Cronin-Golomb, A. Yariv, IEEE J. Quantum Electron. **QE-20**, 1508 (1986)
3. *Photorefractive Materials and Their Applications, I*, edited by P. Günter, J.-P. Huignard, Vol. 62 of Topics in Applied Physics (Springer-Verlag, Berlin, 1989)
4. S. Odoulov, M. Soskin, A. Khyzhnyak, *Optical Coherent Oscillators with Degenerate Four-Wave Mixing* (Harwood Academic Publishers, Chur, London, 1991)
5. L. Solymar, D.J. Webb, A. Grunnet-Jepsen, *The Physics and Applications of Photorefractive Materials* (Oxford, Clarendon Press, 1996)
6. J. Feinberg, R. Hellwarth, Opt. Lett. **5**, 519 (1980)
7. F.T. Arecchi, G. Giacomelli, P.L. Ramazza, S. Residori, Phys. Rev. Lett. **65**, 2531 (1990)
8. S. Liu, G. Indebetouw, J. Opt. Soc. Am. B **9**, 1507 (1992)
9. K. Staliunas, M.F.H. Tarroja, G. Slekys, C.O. Weiss, L. Dambly, Phys. Rev. A **51**, 4140 (1995)
10. C. Denz, M. Schwab, M. Sedlatschek, T. Tschudi, T. Honda, J. Opt. Soc. Am. B **15**, 2057 (1998)
11. P. Mathey, Appl. Phys. B **80**, 463 (2005)
12. P. Mathey, S. Odoulov, D. Rytz, Phys. Rev. Lett. **89**, 053901 (2002)
13. P. Mathey, S. Odoulov, D. Rytz, J. Opt. Soc. Am. B **19**, 2967 (2002)
14. M. Grapinet, P. Mathey, S. Odoulov, D. Rytz, Appl. Phys. B **79**, 345 (2004)
15. A. Bledowski, W. Krolikowski, A. Kujawski, J. Opt. Soc. Am. B **6**, 1544 (1989)
16. P. Mathey, M. Grapinet, H.R. Jauslin, B. Sturman, D. Rytz, S. Odoulov, Eur. Phys. J. D **39**, 445 (2006)